

Measurement of Normal Vectors of the Left Ventricle from Segmented MRI: Comparison of four Practical Methods

A. Amar¹, T. Rachidi¹, L. Coghlan¹, A. Bensaid¹, H. Benjelloun², M. Benomar², and S. Imani³

Abstract

Normal vectors are of primary importance in widely used algorithms for reconstructing surfaces. In cardiology, they are fundamental for accurate measurement of wall thickness, a very important parameter in assessing ventricular function. This paper presents a comparison of four practical methods for computing normal vectors to surfaces of the left ventricle, from segmented MRI. The techniques apply equally well to the right ventricle, and more generally to any surface sampled in terms of digitised outlines. Extensive experiments are performed using (i) known noise-free discrete ellipsoids, (ii) known discrete ellipsoids with noisy surfaces. These experiments are carried under various noise percentages, and inter-slice thickness to determine the most robust and accurate of the suggested methods. The best method is applied to segmented MR images of the human left ventricle.

1 Introduction

This research is part of a project whose primary goal is the development of a precise method for assessing ventricular function and myocardial viability [4, 6, 7, 9, 10, 11, 12] based on the evaluation of ventricular geometry, from data obtained from magnetic resonance images. Precise functional assessment is crucial in defining which patients are operable and likely to benefit from revascularisation surgery, thereby guiding decisions that are critical to patient outcomes. It is also fundamental for determining the right moment for surgical referral without allowing a deterioration of function that can jeopardize the result of surgical treatment.

From data in the form of digitised short axis

¹Computer Science and Mathematics Division, School of Science and Engineering Al-Akhawayn University in Ifrane, PO.BOX 104, Ifrane, 53 000, Morocco, e-mail rachidi@alakhawayn.ma.

²Department of Cardiology, Ibn Sina Hospital, Rabat, Morocco.

³Department of Radiology, Ibn Sina Hospital, Rabat, Morocco.

outlines⁴, the normal vectors are computed. Knowledge of normal vectors allows measurement of principal curvatures and principal directions. This gives very detailed assessment of the local *in vivo* (differential) geometry of the heart, which allows, in particular, more accurate measurement of *wall thickness* than presently used “in plane” methods. The latter do not take into account the inclination of the image plane to the wall. This is especially a problem near the apex of the left ventricle [7, 13]. Accurate information about wall thickness and principal curvatures is essential in quantifying remodeling of the left ventricle due to valvular disease and following myocardial infarction.

2 Previous work

The use of shape for describing 3-D objects has received much attention in the computer vision literature. Several algorithms have been presented [1, 2, 3]. Polynomials are generally used to approximate surfaces. Curvature measures are functions of the partial derivatives of the approximating functions. Since invariant curvature measures are obviously desirable, Gaussian curvature is usually chosen. In cardiac imaging, the methods proposed for approximating surfaces can be divided into two categories: Those that compute directly the parametrisation of the surface from segmented data [8]; and those that first compute the normal vectors, and then deduce the parametrisation of the surface [4, 5]. The latter are intrinsically faster.

In this paper we investigate four methods for approximating the normal vector at a given point on the surface of the left ventricle from its outlines. These methods use local information extracted directly from a neighbourhood of a point under focus to compute the coordinates of the normal vector. The four methods are compared in terms of the angle difference between the *true* normal vectors and the computed ones for **a)** noise-free known ellipsoids, and **b)** known ellipsoids with noisy surfaces. Finally, the best method

⁴Outlines are the result of segmenting MRI images (see Fig. 10).

is applied to segmented MR images of the human left ventricle.

3 Methods

The four methods detailed below are inspired by geometrical properties of smooth surfaces. Assume a global \mathbf{x} - \mathbf{y} - \mathbf{z} coordinate system and a set of outlines, resulting from the segmentation of MR images of the heart as in **Fig. 1**. Each outline O_i is a set of point triplets $P_i(x, y, z)$. Let $P \in O_i$ be a point of interest at which we wish to compute the normal vector \vec{n} .

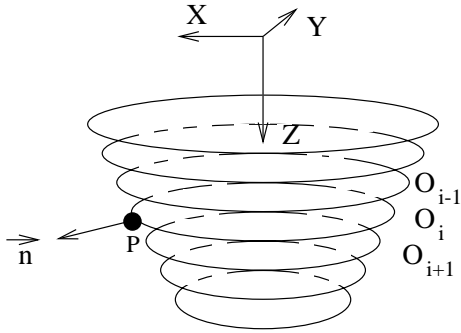


Fig. 1. A set of artificial outlines $\{\dots O_{i-1}, O_i, O_{i+1} \dots\}$ representing segmented MR images of the left ventricle. $P \in O_i$ is the point of interest. \vec{n} is the normal vector to the surface at P .

In the first two methods, a set of r points $S = \{P_1, P_2, \dots, P_r\}$ is chosen from a neighbourhood of P . S is constructed by taking an equal number of neighbouring points from O_i itself, and from the two adjacent outlines (O_{i-1} and O_{i+1}) to O_i . The number of points on each outline (i.e., $r/3$) is a crucial parameter, and is taken into account when evaluating the methods.

3.1 Cross product method (CPM)

This method is derived directly from a geometrical property: the cross product of two vectors \vec{u} and \vec{v} is a vector orthogonal to both \vec{u} and \vec{v} . Consequently the normal at P can be approximated by the following unit vector (see **Fig. 2**):

$$\vec{n} = \frac{\sum_{i=1}^{r-1} (P\vec{P}_i \times P\vec{P}_{i+1})}{\|\sum_{i=1}^{r-1} (P\vec{P}_i \times P\vec{P}_{i+1})\|}$$

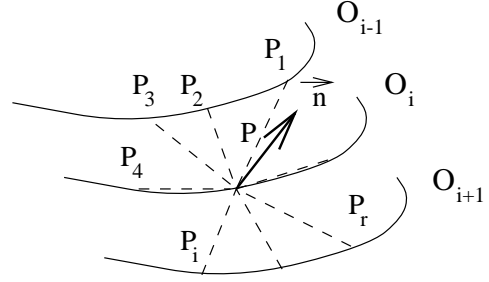


Fig. 2. $P \in O_i$ is the point of interest. $S = \{P_1, P_2, \dots, P_r\}$ is constructed from O_i and neighbouring outlines O_{i-1} and O_{i+1} . S is used to approximate \vec{n} using cross products of vectors $P\vec{P}_i$.

This approach has been used in [4] as an initial approximation.

3.2 Isobarycenter method (IBM)

This technique is based on the assumption that if the set of points S is well distributed, as on a noise-free sphere or paraboloid of revolution, then the normal vector at P lies on the line through P and the isobarycenter point G of S . Formally, let G be the isobarycenter of the set S :

$$\vec{OG} = \frac{1}{r} \sum_{i=1}^r O\vec{P}_i$$

where O is the origin of the coordinate system \mathbf{x} - \mathbf{y} - \mathbf{z} .

The normal \vec{n} is approximated by (see **Fig. 3**):

$$\vec{n} = \frac{P\vec{G}}{\|P\vec{G}\|}$$

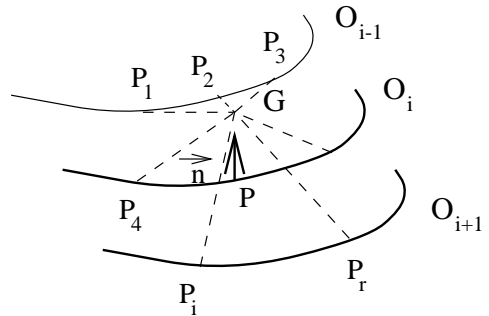


Fig. 3. $P \in O_i$ is the point of interest. \vec{n} is approximated using the isobarycenter point G of S .

3.3 Orthogonal line method (OLM)

Consider a point of interest $P \in O_i$, and the point $P_3 \in O_{i-1}$ such that:

$$\|P\vec{P}_3\| = d = \min_{P_j \in O_{i-1}} \|P\vec{P}_j\|$$

Let $\{P_1, P_2\} \subset O_i$, and $P_4 \in O_{i+1}$ be 3 more points (see Fig. 4) such that:

$$\|P\vec{P}_1\| = \|P\vec{P}_2\| = d, \quad \text{and} \quad \|P\vec{P}_4\| \approx d$$

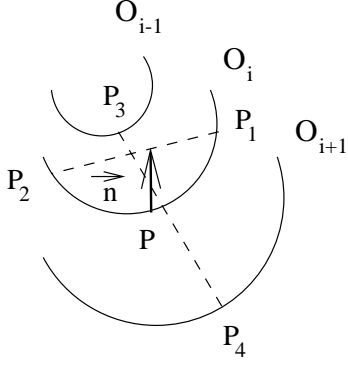


Fig. 4. The four points P_1, P_2, P_3 , and P_4 from neighbouring outlines needed to approximate the normal \vec{n} at P using the orthogonal line method.

The normal \vec{n} can be approximated by the vector based at P that is orthogonal to the two lines: (P_1P_2) and (P_3P_4) :

$$\vec{n} = \frac{P_1\vec{P}_2 \times P_3\vec{P}_4}{\|P_1\vec{P}_2 \times P_3\vec{P}_4\|}$$

3.4 Circles method (CM)

Consider the same points P_1, P_2, P_3 , and P_4 as above. Consider the circle C_1 passing through P, P_1 , and P_2 , and the circle C_2 passing through P, P_3 , and P_4 (see Fig. 5).

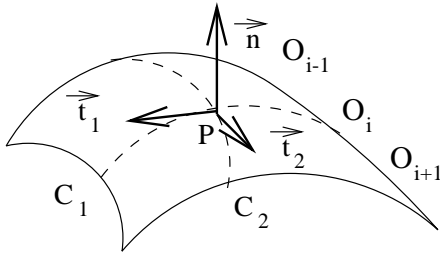


Fig. 5. The tangent vector \vec{t}_1 (resp., \vec{t}_2) to the constructed circle C_1 (resp., C_2), and the resulting approximation of the normal \vec{n} using the circles method.

Let \vec{t}_1 be the tangent vector to C_1 at P and \vec{t}_2 be the tangent vector to C_2 at P . The normal \vec{n} can be approximated by the vector based at P and orthogonal to \vec{t}_1 and \vec{t}_2 :

$$\vec{n} = \frac{\vec{t}_1 \times \vec{t}_2}{\|\vec{t}_1 \times \vec{t}_2\|}$$

4 Evaluation of the methods

Ellipsoids (1) are used to test the four methods. Outlines are constructed by sampling points from the surface of a given ellipsoid.

$$\frac{x^2}{a^2} + \frac{y^2}{b^2} + \frac{z^2}{c^2} = 1 \quad (1)$$

The sampling is such that the resulting outlines are as close as possible to real data obtained from segmented MR images of the left ventricle: points on the outlines are taken at a sampling rate of 3 mm along the arc length to take in consideration the size of the voxels. The coefficients a, b , and c are chosen such that $30 \text{ mm} \leq a = b \leq 50 \text{ mm}$ and $c = 100 \text{ mm}$. A crucial parameter, directly linked to the robustness of the four approaches, is the inter-slice/outline thickness α . Different inter-slice thicknesses $3 \text{ mm} \leq \alpha \leq 10 \text{ mm}$ are considered. The detailed results are presented below.

To evaluate the accuracy of each of the methods on noise-free and noisy outlines, the exact normals are computed, as benchmarks, from the parameters a, b , and c . The average, minimum and maximum angle difference (in degrees) between approximated and theoretical normals, together with standard deviations are computed.

Preliminary tests are performed using noise-free generated outlines to determine the optimal size of the neighbourhood S (optimal value for the parameter r), for CPM and IBM. These tests yielded 15, and 75 respectively as the best size of S . In the subsequent experiments, the size of S is fixed to its optimal value for each of IBM and CPM.

4.1 Discrete noise-free ellipsoids

Table 1 summarises the results obtained for noise-free ellipsoids ($a = b = 30, 40$ and 50 mm , and $c = 100 \text{ mm}$). The total average error in the angle, E_{avg} (in degrees), and the standard deviation σ are computed over all outlines of the ellipsoids.

α	3 mm		6 mm		9 mm	
	E_{avg}	σ	E_{avg}	σ	E_{avg}	σ
CPM	37.68	9.95	13.23	3.32	6.81	3.61
IBM	6.28	1.12	8.31	2.45	10.11	3.30
OLM	27.57	2.81	23.83	3.33	21.65	3.38
CM	27.52	2.78	23.77	3.30	21.59	3.34

Table 1. Total average error E_{avg} and standard deviations σ in degrees for the different methods, on noise-free data for $a = b = 30, 40, 50 \text{ mm}$ and $c = 100 \text{ mm}$, for different inter-slice thicknesses α .

Unexpectedly, the accuracy of all the techniques, but IBM, decreased as the inter-slice thickness decreased. This may be due to the fact that the total average error near the apex outweighs the total average error near the equator, as the inter-slice thickness decreases. Additionally, the total average error per slice E_{avg}/o is significantly smaller for IBM and CPM than for OLM and CM. Moreover, as we move towards the apex, IBM outperforms all the other methods, in particular CPM (see Fig. 6).

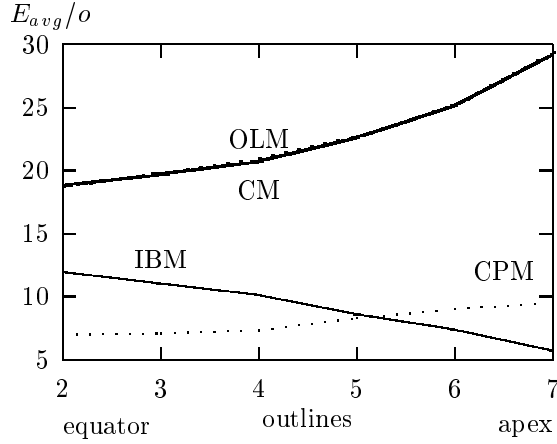


Fig. 6. Average error (in degrees) per outline, as we move from the equator towards the apex, for noise free ellipsoid $a = b = 30$ mm and $c = 100$ mm, for an inter-slice thickness $\alpha = 8$ mm.

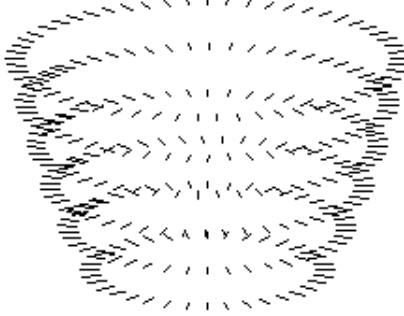


Fig. 7. Normal vectors obtained by IBM for noise-free ellipsoid.

4.2 Discrete noisy ellipsoids

Noisy data are generated by randomly adding noise to noise-free ellipsoids in terms of a percentage of displaced points from their outlines. The error is computed with respect to the normals at the points before adding noise to them. The results of the different methods on ellipsoids with various noise percentages $\epsilon = 10, 20, 30\%$ are summarised in Table 2.

$\epsilon = 10\%$						
α	3 mm		6 mm		9 mm	
	E_{avg}	σ	E_{avg}	σ	E_{avg}	σ
CPM	37.57	17.21	25.30	15.64	23.60	16.62
IBM	6.41	1.05	9.39	8.04	10.64	3.49
OLM	28.09	10.77	24.29	7.60	21.60	5.42
CM	24.97	11.21	23.05	7.46	21.14	5.32

$\epsilon = 20\%$						
α	3 mm		6 mm		9 mm	
	E_{avg}	σ	E_{avg}	σ	E_{avg}	σ
CPM	52.79	18.80	36.96	16.23	32.91	17.92
IBM	6.89	2.88	10.74	12.72	11.83	10.89
OLM	29.92	13.95	24.26	10.19	21.05	6.55
CM	25.09	13.47	22.82	9.24	20.51	6.35

$\epsilon = 30\%$						
α	3 mm		6 mm		9 mm	
	E_{avg}	σ	E_{avg}	σ	E_{avg}	σ
CPM	51.97	18.18	44.52	18.40	40.50	17.63
IBM	7.76	3.59	10.15	10.15	14.29	18.40
OLM	31.75	14.28	23.78	9.58	21.49	7.99
CM	25.49	13.94	21.96	8.87	20.50	7.60

Table 2. Total average error E_{avg} and standard deviations σ in degrees for the different methods, for $a = b = 30, 40, 50$ mm and $c = 100$ mm, for different inter-slice thicknesses α , and various noise percentages $\epsilon = 10, 20, 30\%$.

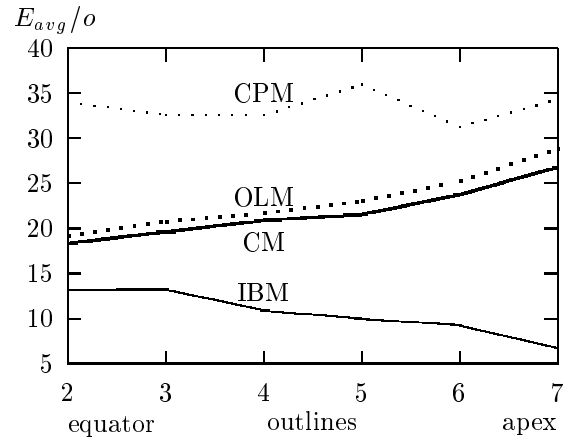


Fig. 8. Average error (in degrees) per outline, as we move from the equator towards the apex, for noisy ellipsoid $a = b = 30$ mm, $c = 100$ mm, and $\epsilon = 20\%$, and for an inter-slice thickness $\alpha = 8$ mm.

Table 2 shows that, as in the case of noise free data, IBM is the only method whose accuracy increases as inter-slice thickness decreases. Furthermore, IBM significantly outperforms all the other methods throughout the whole ellipsoid as shown in **Fig. 8**.

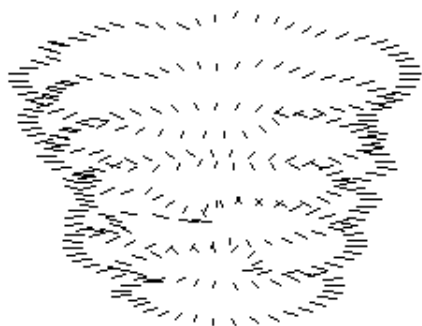


Fig. 9. Normal vectors obtained by IBM for noisy ellipsoid, for $\epsilon = 20\%$.

4.3 Real data from segmented heart MRI

Images are obtained from a 1.5T whole-body MRI Philips system. The final (256×256 pixels, 1024 grey levels) MRI images were segmented by hand⁵ to obtain outlines (see **Fig. 10**). Representative outlines are shown in **Fig. 11**.

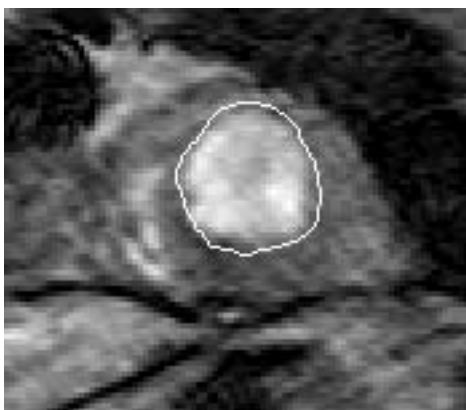


Fig. 10. Example of MRI segmentation.

⁵The segmentation was validated by cardiologists. The authors are currently developing a snake-based automatic segmentation, as part of a cardiac package.

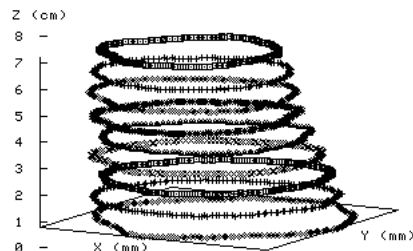


Fig. 11. Left ventricle outlines obtained from segmentation of representative MR images.

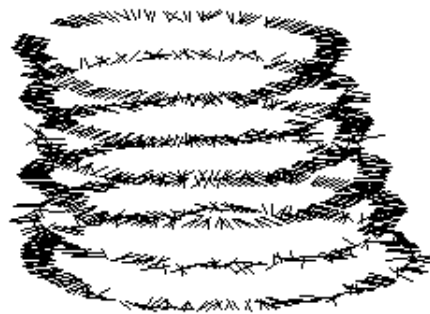


Fig. 12. Normal vectors obtained by IBM for the outlines in **Fig. 11**.

5 Conclusions

The Isobarycenter method significantly outperforms the other methods. However, the total average errors obtained range between 6 and 10 degrees, which we consider not sufficiently accurate for our purpose of accurately quantifying heart geometry. A more refined technique for further improving the measurement of normal vectors is desirable. One approach is to use IBM as the initial approximation for the technique in [4, 5]. The authors are also investigating the use of additional constraints, such as the smoothness of normal vectors along and across outlines, to help in the estimation.

References

- [1] M. Brady and A. Yuille. *An extremum principle for shape from contour*. IEEE Trans. Pattern Anal. Mach. Intell., vol. PAMI-6, pp. 288-301, 1984.

- [2] K. Ikeuchi and B. K. P. Horn. *Numerical shape from shading and occluding boundaries*. Artif. Intell., vol. 19, pp. 141-185, 1981.
- [3] A. P. Wilkin. *Recovering surface shape and orientation from texture*. Artif. Intell., vol. 17, pp. 17-47, 1981.
- [4] L. Coghlan, H. R. Singleton, L. J. Dell'Italia, C. E. Linderholm, G. M. Pohost. *Measurement of three dimensional normal vectors, principal curvatures, and wall thickness of the heart using cine-MRI*. SPIE Medical Imaging, San Diego, CA, SPIE, Vol. 2433, pp. 292-302, 1995.
- [5] L. Coghlan, H. R. Singleton, C. E. Linderholm, G. M. Pohost. *Measurement of normal vectors, principal curvatures, and wall thickness using cine-MRI*. Submitted to PAMI.
- [6] L. J. Dell'Italia, L. Coghlan, H. R. Singleton, G. G. Bladewell, G. M. Pohost. *Curvature-wall Thickness product by magnetic resonance imaging: an index of myocardial adaption to load*. Society of Magnetic Resonance in Medecine. 12th Annual meeting, August, 14-20, New York, N. Y. 1993.
- [7] M. A. Lawson, L. L. Johnson, L. Coghlan, H. R. Singleton, E. L. Tauxe, G. M. Pohost. *End-systolic wall thickness in the assessment of myocardial viability*. International Society of Magnetic Resonance in Medecine. 4th Annual meeting, April 27-May 3, New York, N. Y. 1996.
- [8] E. M. Stokely and S. Y. Wu. *Surface parametrization and curvature measurement of arbitrary 3-D objects: 5 practical methods*. IEEE Trans. Pattern Anal. Mach. Intell., vol. PAMI-8, pp. 833-840, 1992.
- [9] J. Lessick, S. Sideman, H. Azhari, E. Shapiro, J. L. Weiss, and R. Beyar. *Evaluation of regional load in acute ischemia by three-dimensional curvatures analysis of the left ventricle*. Ann. Biomed. Eng. Vol. 21, pp. 147-161, 1993.
- [10] R. C. Semelka, E. Tomei, S. Wagner, J. Mayo, C. Kondo, J. I. Suzuki, G. R. Caputo, and C. B. Higgins. *Normal left ventricular dimensions and function: interstudy reproducibility of measurements with cine-MR imaging*. Radiology 174:763-768, 1990.
- [11] M. C. Dulce, G. H. Mostbeck, K. K. Friese, G. R. Caputo, and C. B. Higgins. *Quantification of the left ventricular volumes and function with cine-MR imaging: comparison of geometric models with three-dimensional data*. Radiology 188:371-376, 1993.
- [12] M. S. Sacks, C. J. Chuong, G. H. Templeton, and R. Peshock. *"In vivo" 3-D reconstruction and geometric characterization of the right ventricular free wall*. Ann. Biomed. Eng., Vol. 21, pp. 263-275, 1993.
- [13] M. A. Lawson, L. L. Johnson, M. Alami, E. L. Tauxe, S. S. Reinert, H. R. Singleton, L. Coghlan, G. M. Pohost. *Correlation of Thallium Uptake with Left Ventricular Wall Thickness by Cine MRI in Patients with*

Myocardial Infarctions. Submitted to Journ. Amer. Coll. Cardiology.